Supporting Information

Orientation Control (Horizontal and Vertical) of TiO_2 Single-Crystalline Nanowire Arrays for High-performance Gas Sensing: A Surface Supersaturation-driven Approach

Chen-Hu Shen,[a,d] Wen-Jing Jiang,[c] Yong-Jun Chen,[a] Guan-E Wang,[a,b] Gang Xu[a,b,] and Xiao-Liang Ye[a,*]*

[a]State Key Laboratory of Structural Chemistry, Fujian Institute of Research on the Structure of Matter, Chinese Academy of Sciences (CAS), 350002, Fuzhou City, Fujian, China.

[b]Fujian College, University of Chinese Academy of Sciences, 350002, Fuzhou City, Fujian, China.

[c]Fujian Science & Technology Innovation Laboratory for Optoelectronic Information of China, 350108, Fuzhou City, Fujian , P. R. China.

[d]University of Chinese Academy of Science (UCAS), Beijing 100049, China.

* Corresponding author.

E-mail: gxu@fjirsm.ac.cn; yexl@fjirsm.ac.cn

Table of Contents

Chemicals

All solvents and reagents obtained from commercial sources were used without further purification. Tetrabutyl titanate (TBT, > 98%) was purchased from General-Reagent. Ethanol (EtOH, AR), sodium chloride (NaCl, AR), hydrochloric acid (HCl, 36 ~ 38%) and N,N-dimethylformamide (DMF, AR) was purchased from Sinopharm Chemical Reagent Co., Ltd. The substrates used to grow nanowire arrays are sapphire substrates ($8 \times 10 \times 0.6$ mm^3) was purchased from Oufeng Optics, China. All aqueous solutions were prepared with Milli-Q water (18.2 MΩ). Ag paste (SA-5121Q) was purchased from Wuhan Youle Optoelectronics Technology Co., Ltd., China, which was used to build the ohmic contact to test the gas sensor.

Preparation of TiO_2 Nanowires

The sapphire substrates were ultrasonically washed with DMF, H_2O and EtOH for 5 min, respectively. The coating colloid solution with ethanol solution of tetrabutyl titanate (TBT) (0.04 M)was coated onto the cleaned sapphire substrate using spin coater at the rate of 3000 rpm for 5 s. They were annealed at 400 ^oC for 30 min to form a layer of TiO_2 seed. Then, the seeded substrate was up-down immersed in 5 mL solution containing de-ionized water, hydrochloric acid, saturated salt water and tetrabutyl titanate (volume ratio of 30 : 15 : 10 : 1) in a Teflon-lined stainless steel autoclave. The autoclave was sealed and maintained at 120 ^oC for 4 hours. After that, the substrate was washed repeatedly with deionized water and ethanol each for 3 times. Finally, the TiO_2 was obtained after heating at 400 ^oC for 30 min. By adjusting the concentration of the crystal seed concentration, TiO_2 NAs with different morphology were achieved. Samples with crystal seed precursor concentration of 0.02, 0.03, 0,04, 0.05 and 0.06 M were labeled **A1**, **A2**, **A3**, **A4** and **A5**, respectively. Sample **A3** was labeled as **TiO_2-H-NAs**, **A5** was labeled as **TiO_2-V-NAs**.

Characterization

Powder X-Ray diffraction (PXRD) patterns of samples were carried out on a Rigaku SmartLab (Japan) equipped with Cu Kα radiation (λ = 1.54060 Å). The scanning electron microscopy (ZEISS Sigma 500) and transmission electron microscope (TEM, JEOL F200) were applied to investigate the morphology of the samples. Raman spectra were obtained on LabRAM HR. The data of XPS were collected on a Thermos Scientific ESCALAB 250 Xi XPS system (monochromatic Al Kα X-rays (1486.6 eV) operating at 15 kV; base pressure: 5.0 $\times 10^{-8}$ Pa). Photoluminescence spectra was performed on a Hitachi F-7100 spectrofluorimeter. A xenon arc lamp (CEL-HXF300/CELHXUV300) with a light filter (200-1000 nm) was utilized as an irradiation source. *In situ* near ambient pressure X-ray photoelectron spectroscopy (NAP-XPS) experiment was carried out with the Proven-X NAP system (Germany, SPECS). The sample of **TiO_2-H-NAs** was exposed to dry air at 5 mbar irradiating by the Xe lamp, and then a gas mixture of 1000 ppm EtOH in air at 5 mbar total pressure irradiating by the Xe lamp.

Gas Sensing Measurement

TiO_2-H-NAs and **TiO_2-V-NAs** were grown on sapphire substrate, which were connected to both ends by a pair of parallel electrodes (silver paste) to fabricate the gas sensor.

The sensor characterization was conducted by a home-made system reported in our previous work.[1] The target gas was introduced into the quartz tube by mixing the certified gas ‘‘mixtures’’ (Beijing Hua Yuan Gas Chemical Industry Co., Ltd., China) and dry air in a proper ratio controlled by the mass flow controllers (CS-200C, Beijing Sevenstar Qualiflow Electronic Equipment Manufacturing Co., Ltd., China) under light irradiation (λ = 200 - 1000 nm) and room temperature. The constant flow was 600 mL min^{-1}, the bias on the sensor was 5 V and the current was recorded using Keithley 2602B Sourcemeter.

The sensor response with positive response in this work is defined as the ratio of sensor resistance in air (R_{air}) and in analytic gas ($R_{analyte}$):

$$\text{Response} = R_{air}/R_{analyte} - 1$$

The sensor response with negative response in this work in this work is defined as the ratio of R_{air} and $R_{analyte}$:

$$\text{Response} = R_{analyte}/R_{air} - 1$$

The response time ($t_{res.}$) of the sensor with positive response is the time required the increasing current to 90% of the saturation value and the recovery time ($t_{rec.}$) is the time required decreasing the saturated current to its 10%. The tres. and trec. of the sensor with negative response is contrary based on the positive response.

The coefficient of variation (CV) is used to represent the change of different cycle on responses, which is defined as:

$$CV = R_{SD}/R_{average} \times 100\%$$

R_{SD} and $R_{average}$ are the standard deviation (SD) and average value of responses with different cycle, respectively.

In order to simulate the ethanol breath test, the dry air was purged into the chamber for stabilizing the base current line. Meanwhile, a mixture of ethanol, carbon dioxide and air with a certain humidity are passed into the gas mixing tank for 15 minutes (See details in the Supporting Video). Subsequently, the mixed gases are purged into the chamber for the sensing test. After a designed response time, the device in the chamber was purged using dry air. In the whole test, the current change of the device in the chamber was monitored by the source meter, which would display on the computer scream.

Raman Spectra Analysis

Rutile TiO_2 was tetragonal and belonged to the space group P42/mnm with two TiO_2 molecules per unit cell.[2] In general, the first-order Raman spectra of rutile TiO_2 exhibits four Fourier Transform (FT) Raman-active fundamental modes corresponding to B_{1g} (143 cm^{-1}), E_g (447 cm^{-1}), A_{1g} (612 cm^{-1}) and B_{2g} (826 cm^{-1}).[3] Besides, it also contained a second-order scattering (*) at 237 cm^{-1}.[4] E_g and A_{1g} were considered as characteristic peaks of rutile TiO_2. The peak of E_g was nonpolar mode, representing the vibration mode of the Ti-O stretch, while A_{1g} was polar modes, indicating the vibration mode of released oxygen atoms from the phase along the c-axis. Raman spectra of TiO_2 was recorded at 532 nm laser at room temperature (Figure S3). Both of them showed four bands, 135 cm^{-1} (B_{1g}) (B_{1g} was relatively small and absent, which related to vibration mode of O-Ti-O bond bending), 258 cm^{-1} (*), 440 cm^{-1} (Eg), and 604 cm^{-1} (A_{1g}) for **TiO_2-H-NAs**, 143 cm^{-1} (B_{1g}), 236 cm^{-1} (*), 445 cm^{-1} (E_g), and 608 cm^{-1} (A_{1g}) for **TiO_2-V-NAs**. **TiO_2-H-NAs** exhibit a slight redshift in the peak position (E_g and A_{1g}) and a slight broadening in linewidth as compared with the **TiO_2-V-NAs** (E_g, full width at half maximum (FWHM) ~ 41 cm^{-1}; A_{1g}, FWHM ~ 36 cm^{-1}), which was likely to be related to a phonon confinement effect and oxygen vacancy defects in rutile TiO_2 structures.[5,6] And the intensity of the Raman peaks related to the concentration or number of molecules. It could be seen from the Figure S3 that the peaks intensity of **TiO_2-H-NAs** was obviously weaker than that **TiO_2-V-NAs**, indicating that **TiO_2-H-NAs** had a smaller thickness, consistenting with the results of Cross-sectional (Figure S1).

Sensing Mechanism

First, when **TiO_2-H-NAs** was exposed to dry air, oxygen molecules were adsorbed on the surface of nanowires and eventually converted to O_2^-(ads) ions by obtaining free electrons from the surface of the nanowires. When the electrons on the surface of the nanowires were consumed, a depletion region was formed near surface of nanowires, resulting in a decrease in the thickness of the conducting channel.

Therefore, the resistance of **TiO_2-H-NAs** in the air environment was very high. When exposed to reducing volatile organic compounds such as ethanol, oxygen ions adsorbed on the surface of nanowires reacted with ethanol, which results to the released of electrons, increased carriers concentration, lowered the width of surface depletion region, increased thickness of conducting channel, and reduced resistance of **TiO_2-H-NAs**.

Demo Experiment

Please find attached videos from BaiduNest Link:

https://pan.baidu.com/s/1X6w7OPg01zBrq35Y4EKR7Q password: tcis

Figure S1

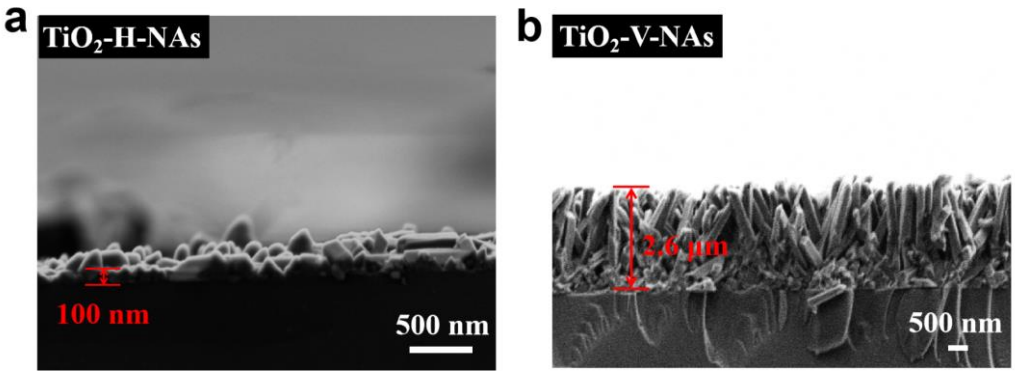

Figure S1 Cross-sectional SEM images of (a) **TiO_2-H-NAs** and (b) **TiO_2-V-NAs**.

Figure S2

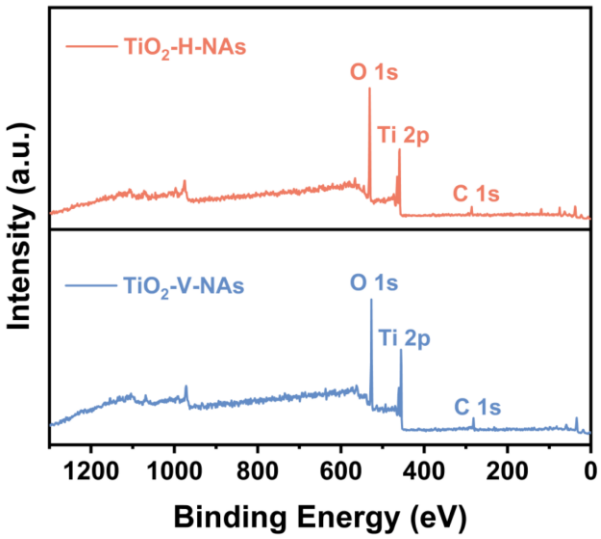

Figure S2 XPS survey spectrum of the **TiO_2-H-NAs** and **TiO_2-V-NAs**.

Figure S3

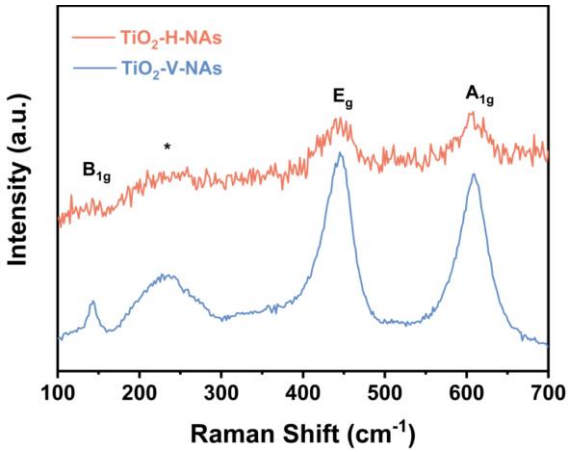

Figure S3 Raman spectra of the **TiO_2-H-NAs** and **TiO_2-V-NAs**.

Figure S4

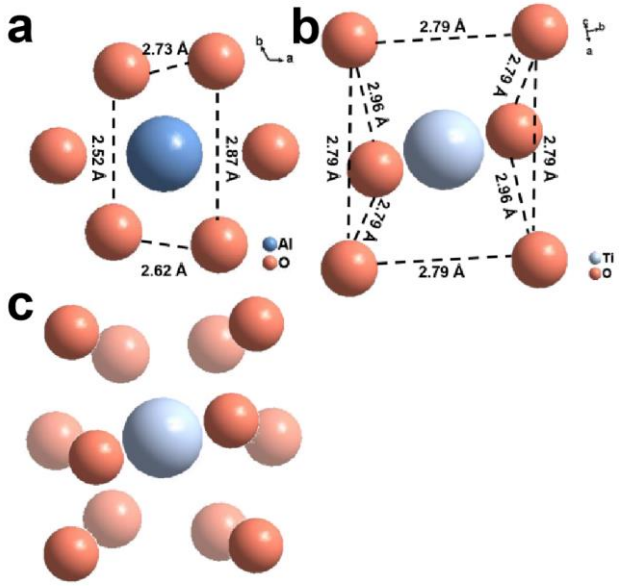

Figure S4 Schematic plots of the lattice relationships between sapphire substrate and **TiO_2-V-NAs**. (a) Sapphire substrate (006), (b) **TiO_2-V-NAs** (101) and (c) **TiO_2-V-NAs** (101) on sapphire substrate (006).

Figure S5

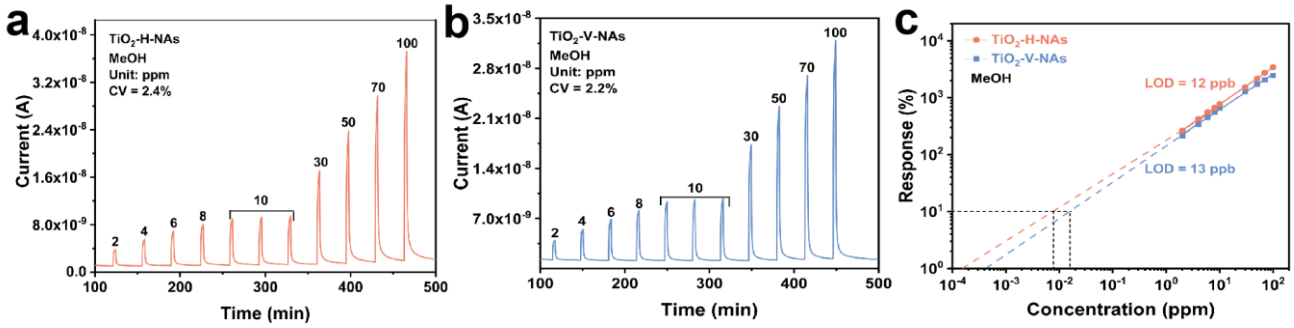

Figure S5 Response-recovery curve to methanol with different concentrations (2-100 ppm) of (a) **TiO_2-H-NAs** and (b) **TiO_2-V-NAs**. (c) Log–log linear fitting of the response-concentration plot for methanol.

Figure S6

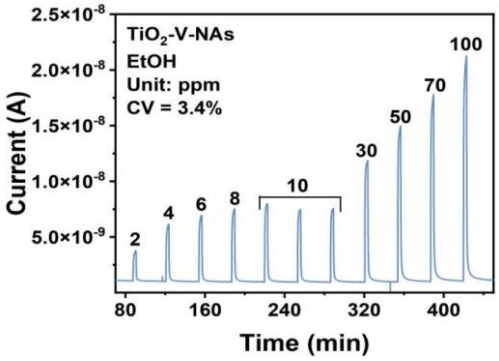

Figure S6 Response-recovery curve to ethanol with different concentrations (2-100 ppm) of **TiO_2-V-NAs**.

Figure S7

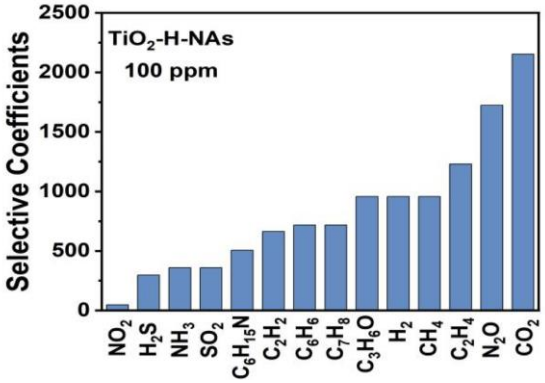

Figure S7 Selectivity coefficients of **TiO_2-H-NAs** to various 100 ppm gases.

Figure S8

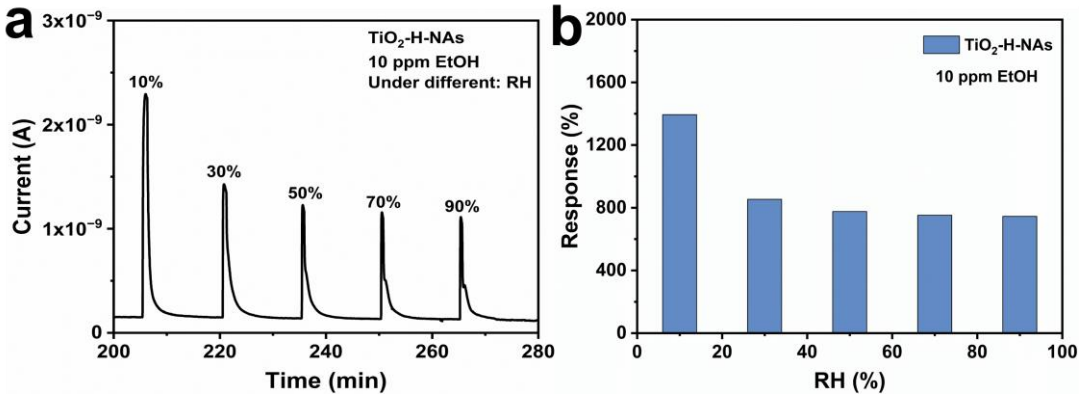

Figure S8 (a) Response-recovery curve of **TiO_2-H-NAs** sensor to 10 ppm EtOH under different humidity condition (10, 30, 50, 70 and 90% RH). (b) Response values of **TiO_2-H-NAs** to 10 ppm EtOH under various RH.

Figure S9

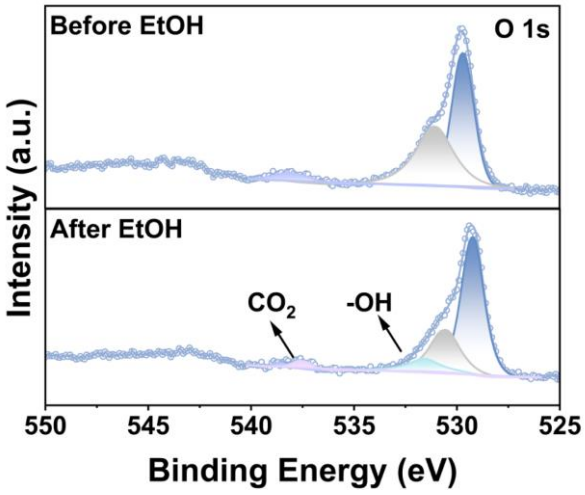

Figure S9 *In situ* NAP-XPS spectra for **TiO_2-H-NAs** of O 1s before (at 5 mbar air) and after (at 5 mbar gas mixture of 1000 ppm EtOH in air) exposure to ethanol.

Table S1

Sensing performance of various chemiresistor gas sensors for ethanol.

No.	Materials	LOD (ppm)	Response Time (s)	Recovery Time (s)	Detection Concentration (ppm)	Ref.
1	WS_2/WO_3	0.001	54	26	10	7
2	TiO_2/TiC	0.01	2	2.2	10	8
3	ZnO oxygen vacant	0.01	300	360	1	9
4	ZnO	0.01	660	720	1	9
5	ZnO/GaN	0.10	12	9	50	10
6	ZIF-8& Ag@SiNWs	0.125	5.5	45	3400	11
7	SnS	0.5	2	3	0.5	12
8	Cubic/orthorhombic SnS	0.5	6	9	10	13
9	$Ti_3C_2T_x/WS_2$	1	9.7	6.6	40	14
10	NiO/SnO_2	1	23	13	100	15
11	TiO_2	1	30	16	100	16
12	g-C_3N_4/GNPs	1	--	--	10	17
13	g-C_3N_4/Ag_2ZrO_3	1	--	--	50	18
14	MoS_2/CeO_2	1	7	5	30	19
15	Ag-doped SnS	1	19	36	10	20
16	Ag-functionalized SnS	1	16	53	10	20
17	$MoO_2/MoO_3/Ti_3C_2T_x$	5	46	276	5	21
18	Graphene-based Ink	5	6	36	30	22
19	TiO_2-$Ti_3C_2T_x$/g-C_3N_4	10	--	--	10	23
20	TiO_2	10	-	--	100	24
21	F-doped SnO_2	10	85	145	100	25
22	APTES-WO_{3-x}	10	168	--	10	26
23	SiO_2/GO	10	--	--	50	27
24	CNTs/Co_3O_4@rGO	10	--	--	50	28
25	α-Fe_2O_3/PANI/PbS	10	--	--	10	29
26	MoO_2-Ni-graphene	15	--	--	1000	30
27	rGO	25	2	17	25	31
28	SnO_2/rGO	29	123	128	145	32
29	PANI/N-doped GQDs	50	80	62	100	33

30	ZnO	50	20	12	100	34
31	Zn-Nitrogenated graphene	50	102	550	1500	35
32	PbS/SnS_2	60	104	84	60	36
33	Au-functionalized PbS/SnS	60	40	65	60	37
34	Poly(o-phenylenediamine)	87	480	1080	130	38
35	AAO	100	--	--	100	39
36	GONRs	100	--	--	100	40
37	$Ti_3C_2T_x$	100	--	--	100	41
38	CuO/C	170	105	18	10	42
39	ZnO/NiO	250	2.7	3.6	250	43
40	$Ti_3C_2T_x$	1000	--	--	1000	44
41	α-Fe_2O_3/Ag	2 mg/L	17	33	35mg/L	45
42	ox-SWCNH/SnO_2/PVP	2 mg/mL	30	50	--	46
43	Ce-doped $LaCoO_3$	10%	16	8	0.3	47
44	TiO_2-V-NAs	0.001	54	60	10	This work
45	TiO_2-H-NAs	0.0006	90	78	10	This work

Notes and References

1 M. S. Yao, W. X. Tang, G. E. Wang, B. Nath, G and Xu, G, *Adv. Mater*., 2016, **28**, 5229-5234.
2 C. R. Aita, *Appl. Phys. Lett.*, 2007, **90**, 213112.
3 V. Swamy, B. C. Muddle and Q. Dai, *Appl. Phys. Lett*., **2006**, *89*, 163118.
4 S. P. S. Porto, P. A. Fleury, and T. C. Damen, *Phys. Rev. Lett.*, 1967, **154**, 522.
5 S. M. Oh and T. Ishigaki, *Thin Solid Films*, **2004**, **457**, 186-191.
6 V. Swamy, *Phys. Rev. B.*, 2008, **77,** 195414.
7 D. Zhang, Y. Cao, J. Wu and X. Zhang, *Appl. Surf. Sci.*, 2020, **503**, 144063.
8 A. V. Raghu, K. K. Karuppanan, J. Nampoothiri and B. Pullithadathil, *ACS Appl. Nano Mater.*, 2019, **2**, 1152-1163.
9 Z. Ul Abideen, J. G. Choi, J. A. Yuwono, A. Kiy, P. V. Kumar, K. Murugappan, W. J. Lee, P. Kluth, D. R. Nisbet, T. Tran-Phu, M. H. Yoon and A. Tricoli, *Adv. Electron. Mater.*, 2023, **9**, 2200905.
10 C. Wang, Z. G. Wang, R. Xi, L. Zhang, S. H. Zhang, L. J. Wang and G. Pan, *Sens. Actuators B Chem.*, 2019, **292**, 270-276.
11 Y. Qui, X. Wang and J. Zang, *Sens. Actuators B Chem.*, 2021, **340**, 129959.
12 Y. Qin, Y. Bai, J. Xie and H. Gui, *Vacuum*, 2023, **207**, 111616.
13 Y. Qin, Y. Liang, C. Zhou and Y. Bai, *Sens. Actuator B Chem.*, 2024, **404**, 135285.
14 W. Y. Chen, X. Jiang, S. N. Lai, D. Peroulis and L. Stanciu, *Nat Commun.*, 2020, **11,** 1302.
15 N. Jayababu, M. Poloju, J. Shruthi and M. V. R. Reddy, *Ceram. Int.*, 2019, **45**, 15134-15142.
16 B. Bhowmik, K. Dutta and P. Bhattacharyya, *IEEE Trans. Electron Devices.*, 2019, **66**, 1063-1068.
17 S. Sahani, S. J. Park, Y. Myung, T. H. Pham,T. T. Tung and T. Y. Kim, *ACS Omrga*, 2022, **7**, 41905-41914.
18 S. P. S. David, S. Veeralakshmi, M. S. Priya, S. Nehru and S. Kalaiselvam, *J. Mater. Sci. Mater. Electron.*, 2022, **33**, 11498-11510.
19 J. Zhang, T. Li, J. Guo, Y. Hu and D. Zhang, *Appl. Surf. Sci.*, 2021, **568**, 150942.
20 Y. Qin and X. Wang, *Physica E low Dimens. Syst. Nanostruct.*, 2021, **131**, 114752.
21 S. Zhang, P. Song, Y. Zheng, Y. Ding and Q. Wang, *J. Alloys Compd.*, 2022, **925**, 166663.
22 K. Hassan, T. T. Tung, P. L. Yap, H. Rastin, N. Stanley, M. J. Nine and D. Losic, *ACS Sens.*, 2021, **6**, 3685-3695.
23 M. Hou, J. Gao, L. Yang, S. Guo, T. Hu and Y. Li, *App. Surf. Sci.*, 2021, **535**, 147666.
24 M. Wang, Y. Zhu, D. Meng, K. Wang and C. Wang, *Mater. Lett.*, 2020, **277**, 128372.
25 E. P. Nascimento, H. C. T. Firmino, A. M. C. Santos, H. B. Sales, V. D. Silva, D. A. Macedo, G. A. Neves and E. S. Medeiros, R. R. Menezes, *J. Am. Ceram. Soc.*, 2021, **104**, 1297-1308.
26 M. Tomic, Z. Fohlerova, I. Gracia, E. Figueras, C. Cane and S. Vallejos, *Sens. Actuators B Chem.*, 2021, **328**, 129046.
27 N. Kaur, M. Singh, A. Casotto, H. M. M. M. Arachchige and L. Sangaletti, E. Comini, *Appl. Phys. Rev.*, 2022, **9**, 041407.
28 M. Morsy, I. S. Yahia, H. Y. Zahran and M. Ibrahim, *J Inorg Organomet Polym Mater.*, 2018, **29**, 416-422.
29 Y. Zhang, W. Pan, G. Dong and D. A. Zhang, *J. Mater. Sci. Mater. Electron.*, 2019, **30**, 17907-17915.
30 S. Mehmood, X. Zhao, M. F. Bhopal, F. U. Khan, Y. Yang, G. Wang and X. Pan, *Appl. Surf. Sci.*, 2021, **554**, 149595.
31 P. Tiwary, S. G. Chatterjee, S. S. Singha, R. Mahapatra and A. K. Chakraborty, *FlatChem*, 2021, **30**, 100317.
32 N. Pienutsa, P. Roongruangsree, V. Seedokbuab, K. Yannawibut, C. Phatoomvijitwong and S. Srinives, *Nanotechnology*, 2020, **32**, 11.

33 C. M. Masemola, N. Moloto, Z. N. Tetana, S. S. Gqoba, P. K. Mubiayi and E. C. Linganiso, *Mater. Chem. Phys.*, 2022, **287**, 126229.
34 P. Tiwary, R. Mahapatra and A. K. Chakraborty, *J. Mater. Sci. Mater. Electron.*, 2019, **30**, 5464-5469.
35 J. Qiu, X. Hu, L. Shi, J. Fan, X. MJin, W. Zhang and J. Wang, *Sens. Actuators B Chem.*, 2021, **392**, 129221.
36 P. S. Kuchi, H. Roshan and M. H. Sheikhi, *J. Alloys Compd.*, 2020, **816**, 152666.
37 H. Roshan, P. S. Kuchi, M. H. Sheikhi and A. Mirzaei, *Mater. Sci. Semicond. Process.*, 2021, **127**, 105742.
38 S. Samanta, P. Roy and P. Kar, *Mater. Sci. Eng. B.*, 2020, **256**, 114541.
39 C. K. Chung and C. A. Ku, *Micromachines*, 2023, **14**, 1330.
40 H. Abdollahi, M. Samkan and M. Bayat, *Mater. Res. Express.*, 2019, **6**, 075053.
41 C. E. Shuck, M. Han, K. Maleski, K. Hantanasirisakul, S. J. Kim, J. Choi, W. E. Reil and Y. Gogotsi, *ACS Appl. Nano Mater.*, 2019, **2**, 3368-3376.
42 H. Lim, H. Kwon, H. Kang, J. E. Jang and J.E. Kwon, *Nano-Micro Lett.*, 2024, **16**, 113.
43 S. T. Hezarjaribi and S. Nasirian, *J Inorg Organomet Polym Mater.*, 2020, **30**, 4072-4081.
44 H. J. Koh, S. J. Kim, K. Maleski, S. Y. Cho, Y. J. Kim, C. W. Ahn, Y. Gogotsi and H. T. Jung, *ACS Sens.*, 2019, **4**, 1365-1372.
45 D. Garcia-Osorio, P. Hidalgo-Falla, H. E. M. Peres, J. M. Goncalves, K. Araki, S. Garcia-Segura and G. Picasso, *Sensors*, 2021, **21**, 440.
46 C. Cobianu, B. C. Serban, N. Dumbravescu, O. Buiu, V. Avramescu, C. Pachiu, B. Bita and M. Bumbac, *Nanomaterials*, 2020, **10**, 2552.
47 L. Wu, X. Shi, H. Du, Q. An, Z. Li, H. Xu and H. Ran, *AIP Adv.*, 2021, **11**, 055305